

Nonlinear beam shaping by a cloud of cold Rb atoms

G. Labeyrie^{1,a}, T. Ackemann^{2,b}, B. Klappauf^{3,c}, M. Pesch^{2,d}, G.L. Lippi^{4,e}, and R. Kaiser^{1,f}

¹ Laboratoire Ondes et Désordre^g, 1361 route des Lucioles, 06560 Valbonne, France

² Institut für Angewandte Physik, Westfälische Wilhelms-Universität Münster, Corrensstraße 2/4, 48149 Münster, Germany

³ Optoelectronics Research Center, University of Southampton, Southampton SO17 1BJ, UK

⁴ Institut Non Linéaire de Nice^h, 1361 route des Lucioles, 06560 Valbonne, France

Received 6 October 2002 / Received in final form 17 December 2002

Published online 18 February 2003 – © EDP Sciences, Società Italiana di Fisica, Springer-Verlag 2003

Abstract. First experimental investigations are reported on nonlinear beam shaping due to the interaction between an intense laser beam and a cloud of laser cooled rubidium atoms. Resonant excitation of the $F = 3 \leftrightarrow F' = 4$ hyperfine transition is considered. The single-pass interaction through the cold vapor causes an increase in the laser beam intensity in the forward direction (zero transverse wavevector component) when observed in Fourier space, for sufficiently high values of saturation. A qualitative explanation of the observations based on a two-level model for a resonantly excited transition proves acceptable. The observations are compatible with an interpretation based on nonlinear index-induced focusing of an incident beam with curved wavefront, as is used in *z-scan* measurements. Simple physical considerations allow us to deduce the conditions for the observability of optical patterns in the beam transmitted by a cold atomic cloud.

PACS. 42.65.Jx Beam trapping, self-focussing, and thermal blooming – 32.80.Pj Optical cooling of atoms; trapping – 42.65.Sf Dynamics of nonlinear optical systems; optical instabilities, optical chaos and complexity, and optical spatio-temporal dynamics

1 Introduction

The spontaneous formation of spatial structures in the interaction between an electromagnetic light field and a nonlinear medium has been observed since the early days of laser physics. The narrow-linewidth, tunable and intense radiation of a laser beam can readily excite a nonlinear response and lead to such a wealth of effects that the whole branch of investigation, called nonlinear optics, was born as a result of the laser's development. Although crucial when feedback is present (*e.g.*, due to a resonant optical cavity), the primary effect of the interaction between a (quasi-) resonant beam and a nonlinear material is already detectable in a single-pass interaction, observing the shape of the beam itself either inside the medium, or after crossing it.

Self-trapping [1–3], and self-focussing [4] were observed in several materials subjected to focussed laser pulses and

various nonlinear phenomena accompanied the appearance of filaments [5]. A wealth of work on damage induced by filamentation appeared very soon because of its practical implications (*cf.* [6, 7] for a comprehensive discussion and a large literature list). A comprehensive review of the early work on self-focussing and self-defocussing – the two effects that could be best described at the time – can be found in [8–11].

The rationale for these investigations is both fundamental (understanding the basics of the beam-matter interaction in an extended system) and applied at the same time. Indeed, searching for ever increasing laser power outputs, one is soon confronted with *distortions* in the laser beam shape that set strong limitations in the upscaling of powerful sources.

Systematic investigations of the properties of optical structures began in the mid-1980's, once the computing power grew sufficiently to allow researchers to simulate the field-matter interaction with enough detail. Several reviews have appeared in the last decade summarizing the state of the understanding of the mechanisms leading to the formation of patterns in the interaction between a laser beam (normally cw) and an optical medium [12–17].

Many schemes have been studied over the years, involving feedback from cavities filled with atomic vapours [18–20], semiconducting materials [21–25],

^a e-mail: Guillaume.Labeyrie@inln.cnrs.fr

^b e-mail: t.ackemann@uni-muenster.de

^c e-mail: bgk@orc.soton.ac.uk

^d e-mail: pematze@zivlnx01.uni-muenster.de

^e e-mail: Gian-Luca.Lippi@inln.cnrs.fr

^f e-mail: Robin.Kaiser@inln.cnrs.fr

^g FRE-2302 CNRS

^h UMR 6618 CNRS-UNSA

photorefractive crystals [26–28], or liquid crystals [29–31]. More complex systems have been devised, *e.g.*, involving a phase conjugate cavity [32,33] or exotic materials [34]. The investigations that have resulted in the best comparison between experiments and a theoretical description are probably those that have been based on feedback from a single mirror [35–39], especially in the case where an atomic vapour is used as the nonlinear medium [17,40–43].

For fundamental investigations, atomic samples have been a preferred choice, since their response to the electromagnetic field can be accurately modeled, their homogeneity is very high, their preparation techniques are standard, and there are no difficulties inherent with fluctuations in composition or quality that are typical of many other samples (*e.g.*, crystals, semiconductors, etc.). However, in the traditional way of preparing the atomic sample for these experiments (atomic jets and cells with or without buffer gas) there are a number of shortcomings: Doppler broadening, multilevel structure, hyperfine substructure, diffusion of atoms (hence of *excitation* outside the interaction region) or of radiation (inelastic scattering), to name only the main ones. These are not necessarily all present simultaneously, but are at the origin of some of the difficulties encountered in comparing experimental results and theoretical models. Indeed, some of these phenomena render the interaction so complex that it is sometimes difficult to obtain a clear picture of the underlying physical mechanisms.

One of the inherent disadvantages coming from these preparation techniques is that the effective loss mechanisms introduced by collisions, Doppler broadening, loss of atoms from the interaction volume (*e.g.*, due to motion), etc., require the use of fairly large amounts of laser power (preferable in a cw regime). Save for a few exceptions [43,44], the agreement between predictions and observations even in experiments using atoms as a nonlinear medium has only been qualitative¹.

Recent progress in the preparation of cold atomic samples has rendered them an attractive alternative for the study of patterns in optics. Their advantages are numerous. The atomic motion, although not entirely removed, does not amount to a substantial perturbation, as atoms are nowadays readily cooled below the Doppler limit. On the electronic relaxation time scale, an alkali atom moving even at speed of 1 m/s moves only by a small fraction of the laser field’s wavelength. Collisions are entirely negligible in typical cold atomic samples and, hence, the transition linewidths are reduced to the spontaneous (radiative) mechanisms.

Besides greatly simplifying the interaction, down to the fundamental physical process (pure levels, limited by spontaneous emission), such narrow linewidths offer the advantage of automatically allowing for the selection of single isotopes – without resorting to costly techniques – and single transitions, even among the wealth of hyperfine levels. Repumping techniques, well developed over the years, allow one to select a chosen transition and operate

with nearly constant population (*i.e.*, atom number) on level combinations of choice: two-, three- or multi-level. Selecting the field polarization appropriately, a wealth of schemes is available to the experimenter.

Nonlinear optical effects in cold vapors have already been studied in pioneering experiments focussing on Raman spectroscopy [45,46], Four Wave Mixing [47,48], Electromagnetic Induced Transparency [49,50], dark states and anomalous dispersion [51,52], squeezing [53], Recoil Induced Resonances [54,55], recoil induced effects in Optical Bistability [56], quantum nondemolition measurement and cavity QED [57–59], and lasing without inversion [60]. A recent review [61] presents the state of the art on nonlinear optics in cold atoms. The issue of strong variations in the speed of light, related to gigantic anomalous dispersion values obtainable in cold samples, has also attracted much attention and strong reductions in the speed of light [62–65] have been observed. The extremely large effects that result from this dispersion allow for the appearance of nonlinear optical effects at very low light levels [66].

On the other hand, we are not aware of published experiments on transverse effects, *i.e.*, self-focusing/defocusing, beam reshaping or optical pattern formation, due to the interaction of a laser with a cold atom cloud. One reason is that very large optical densities are needed to observe any effect (*cf.* Sect. 4) and not many existing setups are capable of providing samples of this kind. This makes the use of cold atomic clouds as a nonlinear medium for these investigations still a challenging experiment more than ten years after the first realization of a magneto-optical trap.

The aim of this paper is to present the first experimental results on transverse effects obtained by shining a laser beam on a sample of cold atoms. Qualitatively, we observe that the transmitted beam’s far field intensity distribution is enhanced on-axis compared to the incident beam. We also observe a smoothing of the intensity distribution in the presence of the cold atoms.

We examine various mechanisms that can be responsible for the observations: the nonlinear response of a two-level system (on- or off-resonance), the resulting (aspheric) lens – assimilating the cloud to a thin medium –, the effects of linear propagation combined with the thin lens (a sort of *z-scan*), and nonlinear propagation through the cloud (dropping the assumption of a thin medium). These considerations allow us to gain a great deal of insight into the mechanisms acting in the system and, in light of finding a *minimal* theoretical description capable of explaining the experimental observations, exclude those effects that cannot be held responsible for the observed results. This contribution, rather than presenting a final answer, opens a new field of investigation and much work remains to be done.

Section 2 presents the experimental setup and the characteristics of the system on which we have carried out the investigation while the observations are reported in Section 3. A simple way of modeling the atomic response to the laser field and obtaining from it the transmission

¹ The situation is even worse for more complex systems (*e.g.*, semiconductors, etc.).

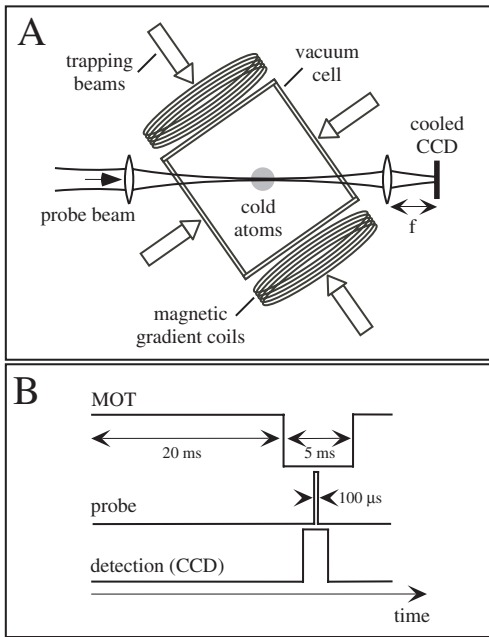


Fig. 1. Scheme of principle of the experimental setup. (a) A standard MOT is prepared with six laser beams split from a same stabilized laser. A probe beam, issued from a separate, frequency stabilized and tunable laser, is focussed onto the atomic sample with the help of a telescope (first lens not shown), down to a beam diameter $\approx 87 \mu\text{m}$ (FWHM) and is detected in the far field with a camera. (b) The preparation phase of the cold atoms is alternated with the measurement phase (no trapping beams or repumper) and takes 20 ms (upper line). In the measurement window (5 ms) a probe beam is applied for a desired, variable, time (center line) and the image is collected by opening the shutter of the CCD camera (bottom line). An image can be acquired over several cycles, depending on the amount of light reaching the CCD under the conditions chosen for the measurement.

function, is reported in Section 4. Section 5 analyses in some detail the effects of the cold cloud, considered as a thin sample, on the Gaussian beam on the basis of different hypotheses: a purely absorptive medium, a purely dispersive one, or a superposition of resonant and non-resonant levels interacting either with a plane phase front or with a curved one. Propagation effects, originating from the thickness of the cloud, are discussed in Section 6. A physical discussion of the results is offered in Section 7. Some conclusions, which include plans for further work and perspectives in the field, close this paper (Sect. 8).

2 Setup and description of the experiment

The experimental setup is illustrated in Figure 1. It consists of a magneto-optical trap (MOT) loaded from a dilute vapor of rubidium 85 atoms [67] (magnetic gradient $\nabla B \approx 7 \text{G/cm}$). Six independent trapping beams are obtained by splitting an initial laser beam slightly detuned to the red of the trapping transition (power per beam 30 mW, beam diameter 2.8 cm (FWHM), rubidium saturation in-

tensity $I_{\text{sat}} = 1.6 \text{mW/cm}^2$, detuned from resonance by $\delta \approx -3\Gamma$ where $\Gamma = 2\pi \times 5.9 \text{MHz}$ is the natural width of the transition). The repumper is obtained by two counter-propagating beams from a free running diode laser tuned to the $F = 3 \rightarrow F' = 3$ transition of the D_2 line. The atomic cloud produced by the MOT has a quasi-Gaussian density profile of diameter $\approx 4 \text{mm}$ FWHM. It contains approximately 3×10^9 atoms, with a spatial density $n_{\text{at}} \approx 4 \times 10^{10} \text{cm}^{-3}$ at the center of the cloud. The corresponding optical thickness of the sample, measured by transmission of a weak and collimated probe, is $b_{\text{res}} \approx 18$ (on resonance: small signal transmission $T = \exp(-18)$). The velocity distribution of the atoms has been measured by a time-of-flight technique to be $v_{\text{rms}} \approx 10 \text{cm/s}$.

To observe the non linear transmission of light, we alternate a transmission phase with a MOT preparation phase. During the transmission phase the MOT (trapping and repumper lasers, magnetic gradient) is switched off and a probe beam is turned on for $100 \mu\text{s}$. Before illumination by the probe beam, most of the atoms are in the $F = 3$ state. The latter is focussed on the cloud with the help of a telescope formed by two $f = 100 \text{mm}$ lenses, to obtain a nominal waist $w_0 = 74 \mu\text{m}$ (*i.e.*, a Gaussian beam with FWHM $87 \mu\text{m}$). The probe beam is close to resonance with the closed trapping transition of the D_2 line: $F = 3 \leftrightarrow F' = 4$. At the end of the transmission phase (duration 5 ms), the MOT is switched on again for 20 ms to recapture the atoms. The transmitted beam far field distribution is recorded by a cooled 16 bit CCD camera (APOGEE, Mod. AP1-0) placed in the focal plane of a converging lens ($f = 300 \text{mm}$). Due to averaging over four pixels, the spatial resolution of the camera is $40 \mu\text{m}$. During the MOT phase, the CCD has to be protected from the intense fluorescence light from the MOT (total radiated power $\approx 4 \text{mW}$). This is accomplished by a synchronized chopper interrupting the detection path. The recapture of the atoms at the end of the measurement interval (Fig. 1b) produces a new atomic sample and a new measurement can be taken. The whole sequence is repeated and integration of the transmitted probe intensity distribution over several repetitions of the measurement is performed for durations varying between 0.25 and 20 s (depending on the amount of incident, and hence transmitted, power).

3 Experimental results

This section is dedicated to presenting the results obtained from the experiment. Throughout this work, the probe beam was kept on resonance with the $3 \leftrightarrow 4'$ transition. Figure 2 shows the evolution of the transmission coefficient of the focussed probe as its intensity is varied. The experimental data (circles) are plotted as a function of the saturation parameter at the center of the beam, defined as $s_0 = I_0/I_{\text{sat}}$, where I_0 is the intensity of the input beam at its center and the saturation intensity is given in Section 2. A simple two-level model-based prediction of the total transmitted power (curve in Fig. 2) shows an

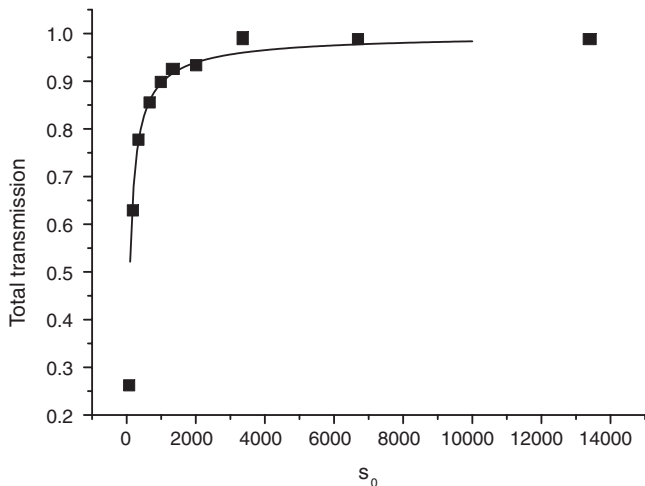


Fig. 2. Comparison between the total transmitted power of a focussed probe for measurements at different values of saturation (where $I_{\text{sat}} = 1.6 \text{ mW cm}^{-2}$) on the beam axis and theoretical predictions. Dots: experimental values; line: theoretical curve based on a two-level model of the transition and an averaged Clebsch-Gordon coefficient.

excellent agreement using an effective Clebsch-Gordon coefficient of 0.7 (accounting for optical pumping leading to a non-uniform distribution of the atoms among the various Zeeman sublevels of $F = 3$). In this model we take into account the spatial dependence of the saturation parameter

$$s(x, y) = \frac{I(x, y)}{I_{\text{sat}}} \quad (1)$$

with larger saturation at the beam center.

Figure 3 shows two examples of shapes for the transmitted beam profile which illustrate the main regimes of interaction. The figures are taken by observing, in the Fourier plane, the beam intensity distribution transmitted by the cloud, from which we have subtracted the incident beam. The operation is performed in order to highlight the (intrinsically small) differences that result from the interaction. Figure 3A shows the transmitted beam at rather low saturation ($s_0 = 50$), where the effect of the cloud is to attenuate the incident field. Figure 3B, corresponding to an intermediate saturation value ($s_0 = 1340$), shows an increase in the transmitted intensity on axis, and close to it. This is also evidenced by the cross-section (lower figure), where a clear enhancement of transmission at low wavenumbers (small θ) can be observed. Figure 3B shows some *noise* both in the 2-D image and in the cross-section. This is due to residual fringes present in the whole optical system (*cf.* the end of this section for a comment on this point).

A systematic study of the power dependence of the beam reshaping was accomplished by varying the probe beam power between $7 \mu\text{W}$ and 2 mW , which correspond to saturation parameter values (on axis) between 50 and 1.3×10^4 , according to the modeling described above (*cf.* Fig. 2). Figure 4 shows the measured transmitted intensity, for different values of saturation, in the form of

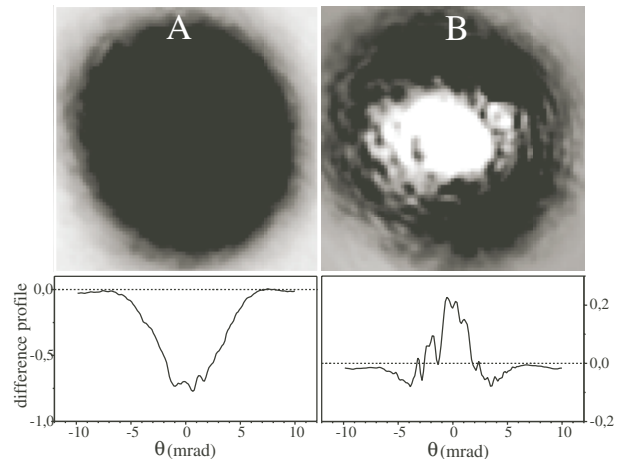


Fig. 3. Transmitted probe intensity distribution detected by the CCD camera in the Fourier plane, after the intensity distribution of the transmitted beam in absence of the cloud was subtracted. The top figures show the 2-D distribution on a grey level scale: white denotes large intensity. The bottom figures show an intensity profile measured by taking a cross-section across the beam. It is normalized to the intensity at zero wavenumber of the incident beam. (A) For low values of saturation ($I/I_{\text{sat}} \approx 50$) absorption dominates (bottom curve), while (B) at higher values ($I/I_{\text{sat}} \approx 1340$) a substantial beam reshaping is visible. In particular, the on axis intensity increases by $\approx 25\%$. In this and the subsequent figures, the beam size is expressed as the divergence angle measured from the $f = 300 \text{ mm}$ lens that transforms the image in the Fourier plane.

cross-sections passing through the beam center. In each case, we show the transmission in the absence (thin line) and in the presence (thick line) of the atomic cloud. At low saturation absorption dominates, but as the probe power increases a clear enhancement of the transmission is visible at beam center (by up to 25%). However, the beam profile remains always monotonic and bell-shaped, and the changes in beam shape (Fig. 3B) amount to a quantitative change in beam width and an increase in intensity near the beam axis. This cannot occur through simple *bleaching* of the transition, nor through acceleration of the atoms through radiation pressure, and strongly suggests the presence of a nonlinear interaction between the probe beam and the cloud.

From the previous figures we notice a considerable reduction in the high frequency components detected in the far field. Figure 5 shows a clear smoothing of the profile induced by the atoms (Fig. 5B, compared to Fig. 5A, obtained in the absence of the cloud). The on-axis cross-sections (lower part of the figure) quantitatively analyse the deviation of the intensity distribution from an ideal Gaussian profile. Besides a slow modulation along the cross-section, attributable to the difference between the actual laser beam and a Gaussian distribution, high frequency spatial components appear. The rms amplitude of this “roughness” is divided by a factor 3.5 in the presence of the cold atoms (Fig. 5B). This effect has been observed systematically throughout the experiment, as shown by

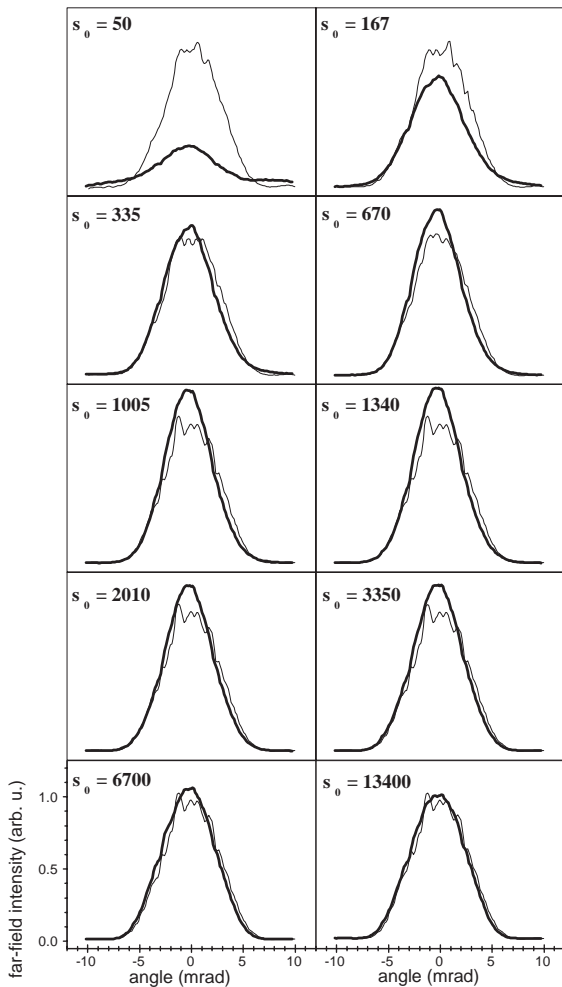


Fig. 4. Radial cross-sections passing through the beam axis for different values of saturation measured by the CCD camera in the absence (thin lines) and in the presence (thick lines) of the atomic cloud.

the profiles of Figure 4, where the solid lines are much smoother than the thin ones (obtained in the absence of the cloud) even at very large saturation values.

Before concluding this overview of the experimental results, we briefly mention other observations made during the measurements, which will be analyzed in the future. Near field measurements (not shown), obtained by imaging the sample on the CCD, also show a certain amount of deformation of the probe beam intensity distribution when the atoms are present. This suggests that propagation plays a not entirely negligible role in the interaction between laser beam and cloud; *i.e.*, a quantitative comparison between predictions and observations will most probably need to include the thickness of the sample. Finally, we have concentrated our attention on the simplest changes in the probe beam transmitted by an ensemble of cold atoms: beam reshaping. However, tuning the probe to a different transition, the $2 \leftrightarrow 1'$, more complex patterns, with multiple rings, appear. They will be the object of investigation in the near future.

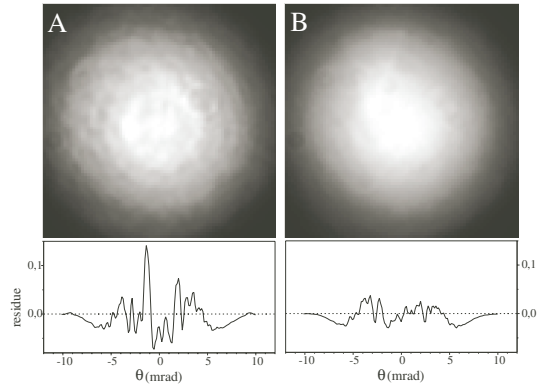


Fig. 5. Transmitted probe intensity distribution in the absence (A) and in the presence (B) of the atomic cloud (for a saturation parameter $s_0 = 13400$). Top figures: 2-D distributions captured by the CCD camera; bottom figures: cross-sections on an axis passing through the beam center, showing the deviation from a Gaussian profile (labelled *residue* in the figure). The fluctuations on cross-section (A) are due to imperfections in the phase front of the incident probe beam. The rms value of these fluctuations is reduced by a factor 3.5 in the presence of the atoms.

4 Description of light-matter interaction

Since the experiment is using a laser beam resonant or quasi-resonant with the $F = 3 \leftrightarrow F' = 4$ transition, one should first examine whether a simple two-level model for this transition is capable of accounting for the experimental observations. This approach is justified by the fact that the spatially averaged transmission properties could be modeled rather nicely within this framework (*cf.* the discussion of Fig. 2 in Sect. 3). However, one should keep in mind that the complete level structure of the rubidium atoms (hyperfine levels and Zeeman sublevels) may play a role, in particular through optical pumping effects. At this stage of description, we choose the simplest physical picture and therefore neglect such effects.

For a description of the electromagnetic field we will assume, throughout the paper, the carrier plane wave component $e^{i(\omega t - kz)}$ to be factored out from the mathematical representation of the field itself and only the slowly varying amplitudes will be retained for the calculations. The propagation of this slowly varying amplitude is governed by the paraxial wave equation [70]. We consider the atomic sample to be transversally uniform, since the size of the cloud (≈ 4 mm) is much larger than the probe's beam waist. In the two-level model with homogeneous broadening, the field's complex transmission coefficient for a thin layer of medium (thickness δz) is given by:

$$t(x, y, z) = \exp \left\{ - \frac{b_{\text{res}} \delta z}{2L} \frac{1 - i \frac{2\delta}{T}}{1 + \frac{(2\delta)^2}{T^2} + s(x, y, z)} \right\}. \quad (2)$$

Here, L is the total thickness of the medium with an optical thickness b_{res} (defined in Sect. 2), $\delta \equiv \omega - \omega_a$, with ω and ω_a laser and atomic frequency, respectively.

The full nonlinear propagation problem will be solved numerically in Section 6. In a first step, we will assume

the medium to be sufficiently thin to neglect any variation due to diffraction taking place during propagation in the shape and size of the beam. Furthermore, supposing that the pump depletion can be neglected, the intensity and the resulting nonlinear transmission coefficient are homogeneous in z and the whole (dispersive and absorptive) action of the medium on the beam can be thought of as taking place at the exit facet. At high saturation values, this assumption holds. As we operate the experiments with large values of s at the beam center, this assumption also remains valid for most of the beam's cross-section. With this assumption and taking $\delta z = L$, the transmission coefficient for the field takes the form:

$$t(x, y) = \exp \left\{ -\frac{b_{\text{res}}}{2} \frac{1 - i\frac{2\delta}{\Gamma}}{1 + \frac{(2\delta)^2}{\Gamma^2} + s(x, y)} \right\}, \quad (3)$$

which provides an intensity coefficient:

$$T(x, y) = |t(x, y)|^2 = \exp \left\{ -b_{\text{res}} \frac{1}{1 + \frac{(2\delta)^2}{\Gamma^2} + s(x, y)} \right\}. \quad (4)$$

Denoting with $I(x, y, z)$ the intensity of the laser beam, the incident field intensity takes the following Gaussian shape:

$$I_{\text{inc}}(x, y, 0) = I_0 e^{-2\frac{x^2+y^2}{w^2}}, \quad (5)$$

where I_0 is the field intensity on axis, and w is the width at the e^{-1} point of the field, measured at the plane of interaction.

The near field distribution of the output field is found by multiplying the input field distribution with the complex transmission coefficient given in equation (3). The field distribution in the far field is obtained by a Fourier transform. This procedure corresponds to the so-called ‘‘thin sample encoding’’ or ‘‘diffraction-free encoding’’ used in [10].

5 Theoretical results: thin medium

In this section, we assume the medium to be *geometrically* thin enough that diffraction effects within the cloud can be neglected. In the first subsection, we assume that the probe's beam waist (*i.e.*, incident plane phase front) and the *thin medium* coincide, while in the second one we allow for an arbitrary amount of curvature of the incident phase front, relative to the medium's position.

5.1 Incident plane phase front

If the phase of the incident field is plane, the input field is given by

$$E(x, y) = E_0 \exp \left(-\frac{x^2 + y^2}{w_0^2} \right), \quad (6)$$

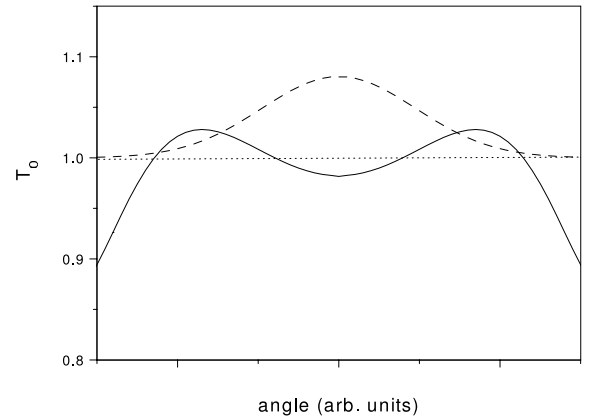


Fig. 6. Far field transmission profile (solid line) along a cut passing through the beam axis for $s_0 = 1000$ considering the interaction with the resonant transition $F = 3 \leftrightarrow F' = 4$. Dashed line: shape of the incident beam intensity (not drawn to scale).

where and $(1/2)\varepsilon_0 c |E_0|^2 = I_0$. As the probe beam is tuned to the resonance of the $F = 3 \leftrightarrow F' = 4$ transition, we first consider a purely absorptive medium, *i.e.* $t(x, y)$ is real. Then the amplitude at zero wavenumber is given by

$$\tilde{E}(0) = \int_{-\infty}^{+\infty} dx dy t(x, y) E_0 \exp \left(-\frac{x^2 + y^2}{w_0^2} \right), \quad (7)$$

where the tilde denotes the Fourier transform. The amplitude of the field at zero wavenumber is obviously reduced by the presence of the transmission function since $t(x, y) < 1$. In Figure 6, we show an example of the profile, obtained as a function of the transverse wavenumber q , for a specific set of parameter values ($b_{\text{res}} = 18$ and $s_0 = 1000$). The figure shows that transmission can increase on the wings. However, on axis it is reduced. On axis the beam experiences attenuation in all cases: at best it could reach total transmission for complete saturation in the beam centre, but never experience an enhancement. This contradicts the experimental observations (*cf.* Figs. 3B and 4). At the end of this subsection we will give a general proof for this statement. Given the fact that pure absorption cannot explain our measurements, we turn to examining whether an off-resonant contribution, which introduces a nonlinear phase shift, could offer an explanation for the observations.

The rather large values of laser intensity applied to the cloud in the experiment suggest that the presence of the $F = 3 \leftrightarrow F' = 3$ transition should be taken into account, although the laser frequency is detuned by $\delta \approx 2\pi \times 120 \text{ MHz} \approx 20\Gamma$. Due to the large values of intensities for which the nonlinear beam deformation is observed, we can consider, in a first approximation, the $F = 3 \leftrightarrow F' = 4$ -transition to be fully saturated and hence – for a qualitative discussion – to be ‘‘non-existent’’. Thus, only the interaction of the laser with the $F = 3 \leftrightarrow F' = 3$ -transition is taken into account. We therefore need to analyse in some detail the interaction between a laser beam

and a strongly off-resonance two-level system. We still consider the medium to be thin.

The off-resonant interaction introduces a nonlinear, position-dependent phase shift, in addition to the attenuation, and it is exactly this phase shift that we intend to explore to see whether it could account for the interference on axis. We write the total phase shift, ϕ_t , defined as the sum of the linear contribution (due to propagation in the medium), ϕ_l , and a nonlinear one coming from the inhomogeneous field intensity distribution in the transverse plane, ϕ_{nl} (for simplicity, only the coordinate of one spatial dimension is written explicitly here):

$$\phi_t = \phi_l + \phi_{nl}, \quad (8)$$

$$= \frac{b_{\text{res}}}{2} \frac{\frac{2\delta}{\Gamma}}{1 + \frac{(2\delta)^2}{\Gamma^2} + s(x)}, \quad (9)$$

where

$$\phi_l = \frac{b_{\text{res}}}{2} \frac{\frac{2\delta}{\Gamma}}{1 + \frac{(2\delta)^2}{\Gamma^2}}, \quad (10)$$

$$\phi_{nl} = -\frac{b_{\text{res}}}{2} \frac{\frac{2\delta}{\Gamma}}{1 + \frac{(2\delta)^2}{\Gamma^2}} \frac{s(x)}{1 + \frac{(2\delta)^2}{\Gamma^2} + s(x)}. \quad (11)$$

The maximum nonlinear phase shift corresponds to high saturation, *i.e.* the condition where the total phase $\phi_t = 0$. This implies that the maximum value of the nonlinear phase shift is equal and opposite to the linear one (Eqs. (9, 10)). For $b_{\text{res}} \approx 18$, a quite substantial maximum value for the nonlinear phase shift is obtained ($\phi_{nl} \approx 4.5$ rad) for $\delta = \pm\Gamma/2$. This value is sufficient for significant beam shaping to occur (*e.g.* [10]). For a detuning of $\delta = 20\Gamma$, one obtains a nonlinear phase shift of $0.0125 b_{\text{res}}$ at high saturation, or $\phi_{nl} \approx 0.22$ rad for $b_{\text{res}} \approx 18$. This is considerably smaller but still clearly nonvanishing.

The result is in itself very interesting, because it provides an estimate of the amount of nonlinear phase shift that can be attained from the cloud. In perspective, such large phase lag values could be used for other experiments, which will be mentioned in the conclusions. However, we now show that by itself this phase shift cannot account for our observations.

Using the transformation

$$\tau = \frac{x^2 + y^2}{w^2}, \quad (12)$$

and equations (1–3), one can quickly obtain the expression for the far field on-axis transmission ($t_0 \equiv t(q=0)$, with q transverse wavevector component)

$$t_0 = \int_0^\infty t(\tau) e^{-\tau} d\tau, \quad (13)$$

where $t(\tau)$ represents the 2-D field transmission function in the near field. In order to evaluate the intensity on-axis component, we write the corresponding expression, which

can be replaced by its majorant, as follows:

$$T_0 = |t_0|^2, \quad (14)$$

$$= \int_0^\infty d\tau t(\tau) e^{-\tau} \int_0^\infty d\tau' t^*(\tau') e^{-\tau'}. \quad (15)$$

Since the latter expression is real and positive, we can rewrite it as

$$T_0 = \left| \int_0^\infty d\tau d\tau' e^{-\tau} e^{-\tau'} t(\tau) t^*(\tau') \right|, \quad (16)$$

$$\leq \int_0^\infty d\tau d\tau' e^{-\tau} e^{-\tau'} |t(\tau) t^*(\tau')|, \quad (17)$$

$$\leq \int_0^\infty d\tau d\tau' e^{-\tau} e^{-\tau'}, \quad (18)$$

$$= 1. \quad (19)$$

This shows that, independently of the value of detuning between field and atomic resonance, the *thin medium approximation* does not explain the observed transmission enhancement on axis, if one restricts the discussion to a two-level medium placed on the waist of the incident beam.

5.2 Incident curved wavefront

In this subsection we will consider the consequences of a phase front curvature of the input beam. For an ideal (parabolic) thin lens it is easy to show, with the help of the ABCD matrices, that the beam's Rayleigh length after the lens depends on the curvature of the phase front of the incident beam. As a general tendency, the Rayleigh length decreases if the wavefront is converging and increases otherwise. Since the amplitude in the far field at zero wavevector is proportional to the Rayleigh length, this implies that an enhancement at zero wavenumber might occur if the wavefront is divergent, *i.e.* if the focus lies before the medium. This dependence of the focusing behaviour on the position of the incident beam waist is used in the so-called *z-scan technique* for a determination of lensing strength and nonlinearity parameters of nonlinear optical materials [69].

If a purely absorptive medium has a Gaussian transmission function, the action of the medium on the beam can also be described by generalized ABCD-matrices, since the beam profile remains Gaussian. However, the focal power parameter is now imaginary [70]. In this case, it is also straightforward to show that the Rayleigh length may become larger than the one of the incoming beam if the incident beam's wavefront is curved. Hence, an enhancement at zero wavenumber might occur. In contrast to the dispersive case, the behaviour is now symmetric with respect to the sign of the curvature.

Since the complex transmission function, equation (3), originating from the saturation of a two-level atom has neither exactly a Gaussian profile, in its real part, nor a parabolic one, in its imaginary part, we are not going to treat in detail these limiting cases, but resort to numerical

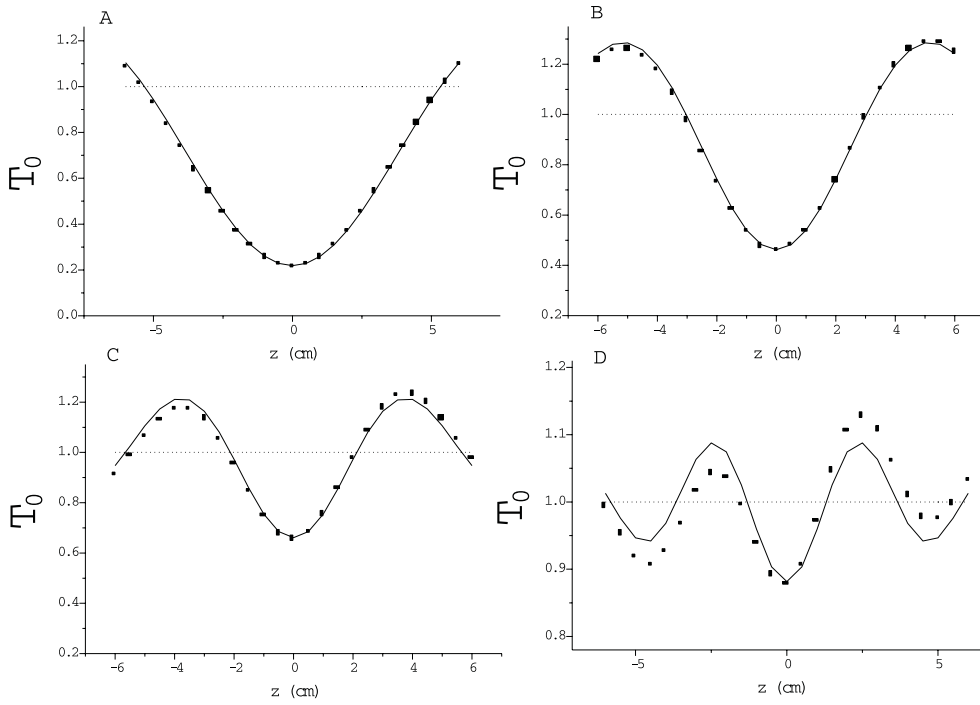


Fig. 7. Interacting probe beam with beam waist offset from the position of the *thin* nonlinear sample. On-axis, far field transmission as a function of position for the $F = 3 \leftrightarrow F' = 4$ transition alone (solid line), or for the superposition of the three resonances: $F = 3 \leftrightarrow F' = 2$, $F = 3 \leftrightarrow F' = 4$ and $F = 3 \leftrightarrow F' = 4$ (dots). The different figures are calculated for s_0 : (A) $s_0 = 100$; (B) $s_0 = 300$; (C) $s_0 = 1000$; (D) $s_0 = 10000$.

simulations which make use of the exact profile. The effect of the neighbouring transitions are included in a straightforward way by adding the associated off-resonant dielectric polarization (a contribution in the form of Eq. (3) with $\delta > 0$ for each transition) to the one originating from the resonant $F = 3 \leftrightarrow F' = 4$ (Eq. (3) with $\delta = 0$) transition.

The numerical evaluation of the transmission in the far field is obtained starting from a full description of the Gaussian beam field distribution using [70]:

$$u(x, y, z) = \sqrt{\frac{2}{\pi}} \frac{1}{w(z - z_0)} \exp \left\{ i \arctan \left(\frac{z - z_0}{z_R} \right) \right\} \times \exp \left\{ -\frac{x^2 + y^2}{w^2(z - z_0)} \right\} \exp \left\{ -ik \frac{x^2 + y^2}{2R(z - z_0)} \right\}, \quad (20)$$

$$w^2(z - z_0) = w_0^2 \left[1 + \left(\frac{z - z_0}{z_R} \right)^2 \right], \quad (21)$$

$$R(z - z_0) = (z - z_0) + \frac{z_R^2}{z - z_0}, \quad (22)$$

$$z_R = \frac{\pi w_0^2}{\lambda} \quad (23)$$

where u represents the normalized Gaussian beam (fundamental mode), w is the beam size at the coordinate z , where the beam waist, of size w_0 , is placed at the coordinate z_0 , and R represents the local radius of curvature of the wavefront. The incident beam is therefore described by:

$$E_{\text{in}}(x, y, z) = A u(x, y, z), \quad (24)$$

where A represents a complex amplitude factor which describes the field's strength.

The transmitted field is therefore of the form (in the near field):

$$E(x, y, L) = A u(x, y, L) t(x, y), \quad (25)$$

where the (complex) transmission function is given by (3). The far field distribution is obtained from equation (25) by Fourier transform.

Figure 7 shows the on-axis component of the far field intensity for different positions of the cloud and for various intensity values of the probe beam. For all intensity values, when the beam waist coincides with the medium there can never be amplification of the on-axis intensity component T_0 . When the beam waist is offset, it is clearly possible to obtain a significant increase for T_0 beyond 1. One can distinguish oscillations in T_0 as a function of the beam waist position, whose amplitude decreases and whose recurrence length decreases with increasing saturation. This figure suggests that an error in placing the incident beam waist of the order of 2 cm could qualitatively reproduce the trend observed in our measurements. The size of such a position mismatch is not incompatible with the precision that could be attained in the probe beam preparation.

The influence of the simultaneous presence of the different transitions ($F = 3 \leftrightarrow F' = 2$, $F = 3 \leftrightarrow F' = 3$, $F = 3 \leftrightarrow F' = 4$), compared to the single $F = 3 \leftrightarrow F' = 4$ transition is displayed in Figure 7 (dots). We most clearly notice the appearance of an asymmetry in the oscillations as a function of the medium's position in Figure 7d, due to the off-resonant (dispersive) character of the interaction with the additional lines. This is not surprising and is a well-known feature of the z -scan technique, which exploits the asymmetric response to obtain information about the nonlinear index of refraction [69].

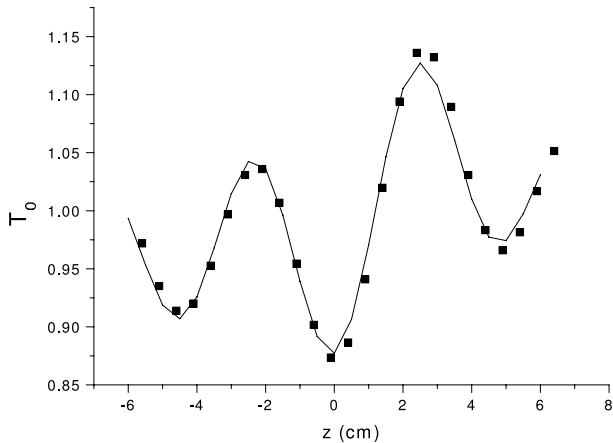


Fig. 8. Inclusion of diffraction inside the cold cloud in the calculation of the far field, on-axis transmission. Without diffraction, as in Figure 7d (solid line), including diffraction over the cloud length included (dots). $s_0 = 10000$.

We remark that the situation considered here differs from the one of CORE (continuous-wave on-resonance enhancement) discussed in [10], since CORE is an enhancement occurring in the near-field (or at a small distance after the medium). Under suitable conditions it is obtained for a plane input phase front and a predominantly absorptive nonlinearity [10]. Hence, the results discussed here and the ones presented in [10] are neither the same nor conflicting: as discussed above, in an absorptive medium the on-axis enhancement in far field occurs only for a curved input phase front, which is not the condition of the CORE experiment [10].

6 Thick medium: propagation effects

As mentioned in Section 3, near field observations hint to the presence of not entirely negligible diffraction effects inside the cloud. Hence, in this section we investigate their influence on the far field transmission on axis.

Numerical simulations of the beam propagation were performed using a conventional split-step beam propagating scheme in the way described in [71] (see also [72]). Diffraction during propagation is described in Fourier space, while the action of the atoms on the light field is calculated in real space. The integration is done on a 256×256 grid in the transverse plane with a longitudinal step size of $5 \mu\text{m}$. Typically, a propagation distance of 4 mm was considered. The atomic sample is assumed to be uniform in the transverse and longitudinal direction. The density is adjusted so that the optical thickness is 18 for a medium length of 4 mm. The beam waist is $w_0 = 74 \mu\text{m}$ and the power is adjusted to achieve the desired saturation level at beam center.

The numerics show that the influence of diffraction within the cold cloud is minimal. In Figure 8, the solid line reports the result of the oscillations in the far field intensity component on axis as a function of the cloud's

position, for the *thin* sample, while the dots give the equivalent result including diffraction over the size of the cloud. We see only minor quantitative differences in the predictions resulting from the two different approaches. We can therefore conclude that the main factor, at least for the parameter values that we have chosen here, is the nonlinear focussing on a curved wavefront.

7 Discussion

Other physical effects, however, are active during the measurement. We have considered the atoms as stationary during the whole interaction. While the assumption is reasonable at the beginning of the interaction (given the slow residual speed, after they have been cooled), radiation pressure accelerates them. One can estimate that during the interaction time the actual acceleration amounts to a Doppler frequency red-shift by about Γ . This implies that the approximation of considering the $3 \leftrightarrow 4'$ level pair as being always on resonance is acceptable only up to a certain point. However, for the parameters of the experiment, the atoms are not pushed so far out of resonance as to become invisible due to power broadening. On the contrary, even on the $F = 3 \leftrightarrow F' = 4$ transition they may be partly contributing with a dispersive part that is opposite to the one estimated for the other transitions. Details about this possible contributions can be experimentally gained only with time resolved measurements (planned for the future). Modeling this effect is not straightforward since it depends on assumptions about the momentum transfer mechanisms. A partial reduction of the weight of this effect comes from hyperfine pumping, which occurs during the measurement window, due to the fact that the repumping beam is turned off. Finally, the atoms that are pushed away from the $3 \leftrightarrow 4'$ resonance interact with a different amount of detuning, which changes in size over time as radiation pressure acts on the cloud. Modeling this component requires also some careful assumptions about the time resolved interaction.

An additional indication that the atoms are not blown away by the probe beam, although intense, comes from the smoothing that we have observed (Fig. 5). Indeed, if the sample were destroyed during the interaction, then one would expect to observe, for increasing saturation, a transmission that resembles more and more closely that seen in the absence of the atoms. Instead, as shown in Figure 4, the smoothing effect persists throughout, suggesting that the “damage” to the cloud imparted by the strong probe is relatively small.

We have numerically investigated the smoothing effect on the transmitted beam in more detail. The incident beam was synthesised by adding to the ideal Gaussian field a spatial “white noise” contribution (limited by the resolution of the numerical discretization) with relative amplitude 15%. The results (Fig. 9) show a strong degree of filtering even at surprisingly large saturation values. The figure shows, in analogy to Figure 4, cuts across a diameter of the far field transmitted intensity distribution.

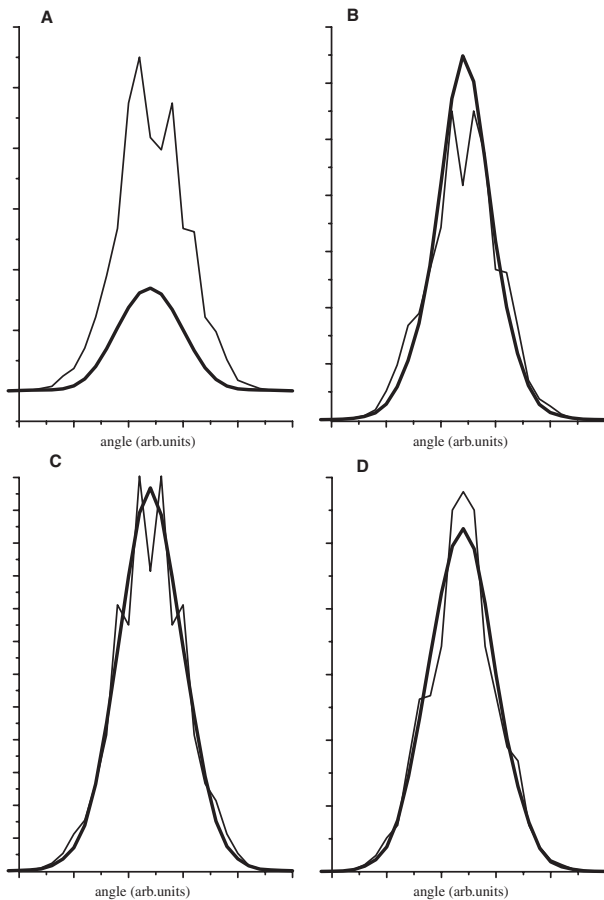


Fig. 9. Numerical profiles evaluated, with the addition of noise in the far field. Incident beam (thin line) without cloud and profile transmitted by the cloud (thick line) for: (A) $s_0 = 50$; (B) $s_0 = 1000$; (C) $s_0 = 2000$; (D) $s_0 = 10000$. The filtering action is remarkable.

The filtering effect is dramatic and qualitatively agrees with the experimental observations (Figs. 4 and 5).

A possible qualitative explanation for such a remarkable filtering action is based on a nonlinear, radially inhomogeneous aperture reminiscent of an apodizing filter, which is self-induced by the laser beam and is due to the strong saturation and bleaching in the beam center imposed on the medium. Transverse spatial frequency components in the near field (where filtering takes place) which produce noise in the far field distribution are located in the wings of the near field profile. Those components that are placed far in the wings of the (near field) intensity profile, so that their saturation level is still very small (s_0 smaller, or of the order of 1), will be absorbed by the optically thick cloud and will therefore be filtered out. All other components, closer to the beam axis, remain substantially unaltered.

8 Conclusions

We presented experimental observations of nonlinear beam reshaping due to the interaction with a laser-cooled

atomic cloud of large optical thickness. The main features are: an enhancement of the far field transmission on axis and a substantial smoothing of the incident beam profile.

An explanation of these effects based on a *thin sample approximation* is not capable of accounting for the observed enhancement, independently of the absorptive or dispersive nature of the interaction, if the incident beam's waist coincides with the medium. On the other hand, inclusion of a wavefront curvature for the incoming wave allows for a qualitative interpretation of our results. This is strongly reminiscent of the well-known *z-scan* technique, used to measure the nonlinear index of refraction of any sample. The observed smoothing of the wavefront is also explained in our numerical approach as a nonlinear filtering introduced by the Gaussian shape of the saturation parameter.

In perspective, we are intending to widen the scope of our investigations by studying in detail the interaction with different transition schemes and incident beam characteristics. One of our aims is to achieve the correct conditions to study the formation of optical structures in the presence of a feedback mirror [17,35,36].

Side issues, that can be addressed, involve the extension of these studies to very dense samples, such as condensates, where the usual approximation of dilute medium – otherwise excellently satisfied – breaks down.

The support of the CNRS and the PACA Region, which allowed the construction of the optical trap, is gratefully acknowledged. T. Ackemann is grateful to the Alexander-von-Humboldt Foundation for financial support.

References

1. M. Hercher, J. Opt. Soc. Am. **54**, 563 (1964)
2. R.Y. Chiao, E. Garmire, C.H. Townes, Phys. Rev. Lett. **13**, 479 (1964)
3. E. Garmire, R.Y. Chiao, C.H. Townes, Phys. Rev. Lett. **16**, 347 (1966)
4. P.L. Kelley, Phys. Rev. Lett. **15**, 1005 (1965)
5. R.R. Alfano, S.L. Shapiro, Phys. Rev. Lett. **24**, 592 (1970)
6. E.L. Kerr, Phys. Rev. A **4**, 1195 (1971)
7. E.L. Kerr, Phys. Rev. A **6**, 1162 (1972)
8. J.H. Marburger, Prog. Quant. Electron. **4**, 35 (1975)
9. Y.R. Shen, Prog. Quant. Electron. **4**, 1 (1975)
10. M. Le Berre, E. Ressayre, A. Tallet, K. Tai, H.M. Gibbs, M.C. Rushford, N. Peyghambarian, J. Opt. Soc. Am. B **1**, 591 (1984)
11. M. Le Berre, E. Ressayre, A. Tallet, F.P. Mattar, J. Opt. Soc. Am. B **2**, 956 (1985)
12. N.B. Abraham, W.J. Firth, J. Opt. Soc. Am. B **7**, 951 (1990)
13. L.A. Lugiato, Phys. Rep. **219**, 291 (1992)
14. N.N. Rozanov, *Transverse Patterns in Wide-Aperture Nonlinear Optical Systems*, Progress in Optics XXXV, edited by E. Wolf (North Holland, Amsterdam, 1996)
15. L.A. Lugiato, M. Brambilla, A. Gatti, Adv. At. Mol. Phys. **40**, 229 (1999)
16. F.T. Arecchi, S. Boccaletti, P.L. Ramazza, Phys. Rep. **318**, 1 (1999)
17. T. Ackemann, W. Lange, Appl. Phys. B **72**, 21 (2001)

18. J. Nalik, L.M. Hoffer, G.L. Lippi, Ch. Vorgerd, W. Lange, *Phys. Rev. A* **45**, R4237 (1992)
19. P. La Penna, G. Giusfredi, *Phys. Rev. A* **48**, 2299 (1993)
20. G.L. Lippi, T. Ackemann, L.M. Hoffer, W. Lange, *Chaos, Solitons, Fractals* **4**, 1409 (1994)
21. W.J. Firth, E.M. Wright, *Opt. Commun.* **40**, 233 (1982)
22. A.V. Grigor'yants, I.N. Dyuzhikov, *J. Opt. Soc. Am. B* **7**, 1303 (1990)
23. V.B. Taranenko, I. Ganne, R.J. Kuszelewicz, C.O. Weiss, *Phys. Rev. A* **61**, 063818 (2000)
24. R. Kuszelewicz, I. Ganne, I. Sagnes, G. Sleky, *Phys. Rev. Lett.* **84**, 6006 (2000)
25. T. Ackemann, S. Barland, J.R. Tredicce, M. Cara, S. Balle, R. Jäger, P.M. Grabherr, M. Miller, K.J. Ebeling, *Opt. Lett.* **25**, 814 (2000)
26. F.T. Arcelli, G. Giacomelli, P.L. Ramazza, S. Residori, *Phys. Rev. Lett.* **65**, 2531 (1990)
27. D. Hennequin, L. Dambly, D. Dangoisse, P. Glorieux, *J. Opt. Soc. Am. B* **11**, 676 (1994)
28. W. Królikowski, M. Saffman, B. Luther-Davies, C. Denz, *Phys. Rev. Lett.* **80**, 3240 (1998)
29. M. Kreuzer, W. Balzer, T. Tschudi, *Appl. Opt.* **29**, 579 (1990)
30. M. Kreuzer, H. Gottschilk, T. Tschudi, R. Neubecker, *Mol. Cryst. Liq. Cryst.* **207**, 219 (1991)
31. M. Kreuzer, H. Gottschling, R. Neubecker, T. Tschudi, *Appl. Phys. B* **59**, 581 (1994)
32. G.C. Valley, G.J. Dunning, *Opt. Lett.* **9**, 513 (1984)
33. D.K. Korwan, G. Indebetouw, *Opt. Commun.* **119**, 305 (1995)
34. B. Fischer, O. Werner, M. Horowitz, A. Lewis, *Appl. Phys. Lett.* **58**, 2729 (1991)
35. G. D'Alessandro, W.J. Firth, *Phys. Rev. Lett.* **66**, 2597 (1991)
36. G. D'Alessandro, W.J. Firth, *Phys. Rev. A* **46**, 537 (1992)
37. R. Macdonald, H.-J. Eichler, *Opt. Commun.* **89**, 289 (1992)
38. T. Honda, H. Matsumoto, *Opt. Lett.* **20**, 1755 (1995)
39. C. Denz, M. Schwab, M. Sedlatschek, T. Tschudi, T. Honda, *J. Opt. Soc. Am. B* **15**, 2057 (1998)
40. G. Giusfredi, J.F. Valley, R. Pon, G. Khitrova, H.M. Gibbs, *J. Opt. Soc. Am. B* **5**, 1181 (1988)
41. G. Grynberg, A. Maître, A. Petrossian, *Phys. Rev. Lett.* **72**, 2379 (1994)
42. T. Ackemann, W. Lange, *Phys. Rev. A* **50**, R4468 (1994)
43. T. Ackemann, Y. Logvin, A. Heuer, W. Lange, *Phys. Rev. Lett.* **75**, 3450 (1995)
44. A. Aumann, E. Große Westhoff, R. Herrero, T. Ackemann, W. Lange, *J. Opt. B: Quant. Semiclass. Opt.* **1**, 166 (1999)
45. D. Grison, B. Lounis, C. Salomon, J.Y. Courtois, G. Grynberg, *Europhys. Lett.* **15**, 149 (1991)
46. M. Hennrich, T. Legero, A. Kuhn, G. Rempe, *Phys. Rev. Lett.* **85**, 4827 (2000)
47. J.W. Tabosa, S.S. Vianna, F.A.M. de Oliveira, *Phys. Rev. A* **55**, 2968 (1997)
48. J. Zachorowski, T. Brzozowski, T. Palasz, M. Zawada, W. Gawlik, *Acta Phys. Pol. A* **101**, 61 (2002)
49. M. Mitsunaga, M. Yamashita, H. Inoue, *Phys. Rev. A* **62**, 013817 (2000)
50. G.C. Cardoso, J.W.R. Tabosa, *Phys. Rev. A* **65**, 033808 (2002)
51. G. Wařik, W. Gawlik, J. Zachorowski, Z. Kowal, *Phys. Rev. A* **64**, 051802 (2001)
52. A.M. Akulshin, S. Barreiro, A. Lezama, *Phys. Rev. Lett.* **83**, 4277 (1999)
53. A.Z. Khoury, T. Coudreau, C. Fabre, E. Giacobino, *Phys. Rev. A* **57**, 4770 (1998)
54. J.-Y. Courtois, G. Grynberg, B. Lounis, P. Verkerk, *Phys. Rev. Lett.* **72**, 3017 (1994)
55. C.P. Search, P.R. Berman, *Phys. Rev. A* **63**, 063411 (2001)
56. R. Bonifacio, B.W.J. McNeil, N. Piovella, G.R.M. Robb, *Phys. Rev. A* **61**, 023807 (2000)
57. D.W. Vernooy, A. Furusawa, N.Ph. Georgiades, V.S. Ilchenko, H.J. Kimble, *Phys. Rev. A* **57**, R2293 (1998)
58. J.-F. Roch, K. Vigneron, Ph. Grelu, A. Sinatra, J.-Ph. Poizat, Ph. Grangier, *Phys. Rev. Lett.* **78**, 634 (1997)
59. G.T. Foster, L.A. Orozco, H.M. Castro-Beltran, H.J. Carmichael, *Phys. Rev. Lett.* **85**, 3149 (2000)
60. J. Kitching, L. Hollberg, *Phys. Rev. A* **59**, 4685 (1999)
61. G. Grynberg, C. Robillard, *Phys. Rep.* **355**, 335 (2001)
62. L.V. Hau, S.E. Harris, Z. Dutton, C.H. Behroozi, *Nature* **397**, 594 (1999)
63. M.M. Kash, A. Sautenkov, A.S. Zibrov, L. Hollberg, G.R. Welch, M.D. Lukin, Y. Rostovtsev, E.S. Fry, M.O. Scully, *Phys. Rev. Lett.* **82**, 5229 (1999)
64. D. Budker, D.F. Kimball, S.M. Rochester, V.V. Yashchuk, *Phys. Rev. Lett.* **83**, 1767 (1999)
65. C. Liu, Z. Dutton, C.H. Behroozi, L.V. Hau, *Nature* **409**, 490 (2001)
66. S.E. Harris, L.V. Hau, *Phys. Rev. Lett.* **82**, 4611 (1999)
67. Cf. collective volume: *Laser Manipulation of Atoms and Ions*, edited by E. Arimondo, W.D. Phillips, F. Strumia (North Holland, Amsterdam, 1992)
68. G. Labeyrie, Ch. Miniatura, R. Kaiser, *Phys. Rev. A* **64**, 033402 (2001)
69. M. Sheik-Bahae, A.A. Said, T.-H. Wei, D.J. Hagan, E.W. van Stryland, *IEEE J. Quant. Electron.* **QE-26**, 760 (1990)
70. A.E. Siegman, *Lasers* (University Science Books, Mills Valley, CA, 1986)
71. J.P. Fève, J.J. Zondy, B. Boulanger, R. Bonnenberger, X. Cabriol, B. Ménaert, G. Marnier, *Opt. Commun.* **161**, 359 (1999)
72. L. Thylén, *Opt. Quantum Electron.* **15**, 433 (1983)